ARCHIVES
of
FOUNDRY ENGINEERING

Study on Ladle Baking Process with Oxygen-fuel Combustion

Xiaoyao Wang [a], Guangqiang Liu [a, *], Yuanxin Liu [a], Jian Wang [b]
[a] Liaoning University of Science and Technology, China
[b] Technology Research Center of Bengang, China
* Corresponding author: E-mail address: lgqiang0305@sina.com

Abstract

Oxygen-fuel combustion instead of air combustion for ladle baking has gradually become a new technology for ladle heating in the iron and steel industry. The optimization of oxygen-fuel burner structure is of great significance for the wide application of oxygen-fuel combustion technology in iron and steel enterprises. In this study, a three-dimensional model of 100 ton ladle was established by using the numerical simulation software FLUENT 21.0. The fluid flow, combustion and heat transfer in the process of ladle oxygen baking were studied. The ladle baking effects of four different gas pipeline diameters and four different gas nozzle spacing were compared. The results show that when the gas flow rate and oxygen flow rate are about 1:1, the roasting effect is the best. When the distance between fuel gas nozzle and oxygen nozzle is 150mm~175mm, the baking effect of ladle bottom and wall is better. When the diameter of gas pipe is 150mm, the diameter of oxygen pipe is 60mm, and the distance between gas nozzle and oxygen nozzle is 150mm, the baking efficiency can reach 24.33%. The relevant research provides the basis for the application of oxygen-fuel combustion technology in 100t ladle.

Keywords: Ladle baking, Oxy fuel, Gas diameter, Nozzle spacing

1. Introduction

The steel ladle serves as a pivotal piece of equipment within the refining furnace of the metallurgical industry. The process is primarily categorized into online and offline baking, with its fundamental operating principle revolving around the high-temperature flue gas produced by combustion within the burner. This gas then flows into the ladle and undergoes a heat exchange process, effectively heating up the ladle. Its primary function is to refine the steel contained within, eliminating impurities from the liquid steel while also possessing a certain degree of smelting capability [1-2]. Baking a ladle significantly impacts its thermal state and, consequently, the temperature of the molten steel. Enhancing the preheating effect can elevate the temperature of the ladle lining, thereby mitigating the rate of temperature decline in the molten steel and ensuring uniformity in its temperature[3].

Given the national emphasis on enhancing the quality and reducing the cost of steel products, stricter requirements have been imposed on the temperature control and energy consumption during ladle baking. On the one hand, it is imperative to uniformly bake the ladle to temperatures exceeding $1000\,℃$, and on the other, the baking process must embody energy efficiency, minimal environmental impact, as well as low emissions of carbon, nitrogen oxides, and other detrimental gases [4].

Currently, the primary combustion technique employed for ladle baking is air combustion, a widely adopted practice across the metallurgical industry. However, the flames generated by air combustion are inherently unstable, leading to prolonged baking durations and frequent occurrences of issues like inadequate mixing and incomplete combustion[5-6]. The nitrogen in the air also gets heated and carries the energy from the combustion process along with the hot flue gases out of the steel ladle[7-8]. Simultaneously, the significant quantities of CO_2 and NO_x emitted

lead to severe environmental pollution [9-11]. To address the aforementioned issues, the adoption of oxygen-fuel combustion for ladle baking, as a replacement for traditional air combustion, has gradually emerged as an innovative technology for ladle heating processes. Oxygen-fuel combustion pertains to utilizing oxygen with an oxygen volume fraction Φ (O_2) exceeding 90% as the primary supporting gas. Compared to air-assisted combustion, oxygen-fuel combustion has better flame stability and no additional impurities (such as N_2) input, which can reduce 79% of the heat loss carried away by N_2, significantly increasing the combustion intensity of the fuel and achieving better energy-saving effects[12], This technology is widely regarded as holding immense potential in mitigating NO_x emissions, recycling CO_2 for productive use, and alleviating the greenhouse effect [13-15].

Over the past few decades, extensive research has been undertaken by scholars on the subject of oxygen-fuel combustion. Maia B. conducted an exhaustive study on the combustion of solid fuels utilizing oxygen-fuel combustion. The findings uncovered that, in stark contrast to air combustion, the employment of oxygen-fuel combustion markedly reduces NO_x emissions by an impressive margin of approximately 70% to 80% [16]; LUO conducted research on an air separation unit specifically designed to guarantee a consistent supply of pure oxygen for the combustion process during pure oxygen-assisted combustion, thereby enhancing the efficiency and safety of the operation[17]; GAO devised an innovative oxygen-fuel combustion circulating fluidized bed boiler, with findings suggesting that the employment of pure oxygen significantly diminishes overall energy consumption and curtails CO_2 capture expenses [18]; SHI delved into the combustion behavior of methane in an oxygen-fuel combustion scenario, employing a rapid mixing tubular flame burner. Their investigation revealed that, at a fixed overall flow rate, the mixing combustion process attains its fastest pace when the inlet velocities of both the fuel gas and oxygen are maintained at an equivalent level[19]; ZHUANG meticulously investigated the influence of a pure oxygen lance on the preheating temperature of scrap within a ladle. The findings revealed a discernible trend: as the gas flow rate escalated, the internal annular combustion zone progressively expanded, accompanied by a consistent reduction in the bottom cold zone. Furthermore, the average temperature of the scrap steel consistently climbed upwards [20].

However, the application of pure oxygen-assisted combustion technology in steel ladle baking is limited. Hence, conducting research into fluid dynamics, combustion processes, and heat transfer mechanisms during the pure oxygen-assisted baking of steel ladles, while meticulously examining the influence of varying fuel gas nozzle diameters and nozzle spacings on baking efficiency, can furnish a solid foundation for the implementation of pure oxygen-assisted combustion technology in steel ladle preheating practices. This research holds significant guiding implications for the application of oxygen-fuel combustion technology within steel enterprises.

2. Modeling

2.1. Mathematical model

During the combustion process, there are interactions involving fluid flow, heat transfer, mass transfer, and chemical reactions. Therefore, it is necessary to establish corresponding mathematical models to quantitatively describe the turbulent mean flow field. The main control equations for this simulation are shown below.

Mass conservation equation[21]:

$$\frac{\partial \rho}{\partial t} = -\text{div}\left(\rho \, \vec{v}\right) \tag{1}$$

Conservation of momentum equation[21]:

$$\frac{\partial(\rho \vec{v})}{\partial t} + \text{div}\left(\rho \vec{v} \, \vec{v}\right) = \text{div}\left(\eta \text{grad} \, \vec{v}\right) + \rho \, \vec{g} - \nabla p \tag{2}$$

The conservation of energy equation[21]:

$$\frac{\partial(\rho T)}{\partial t} + \text{div}\left(\rho \vec{v} \, T\right) = S_T + \text{div}\left(\frac{\lambda}{c_p} \text{grad} T\right) \tag{3}$$

Component transportation equations:

$$\frac{\partial \rho c_s}{\partial t} + \text{div}(\rho c_s) = \text{div}[D_s \text{grad}(\rho c_s)] + S_s \tag{4}$$

Where: ρ is the density of the fluid, t is the time, $\vec{v}$ is the velocity vector, η represents dynamic viscosity. p is the pressure, T is the temperature, S_T represents the internal heat source of the fluid, λ is the thermal conductivity, C_p represents specific heat capacity at constant pressure, C_s is the volumetric concentration of the component s, and D_s is the diffusion coefficient of the component s. S_s represents the source term, which is the amount of component s produced per unit volume per unit time through chemical reactions.

The turbulence model adopts the realizable k-ε model, which assumes that the flow field is all turbulent flow and ignores the viscous effect between fluid molecules, with strong applicability and reasonable calculation accuracy, and the specific equations are shown below[20]:

$$\frac{\partial(\rho k)}{\partial t} + \frac{\partial(\rho k u_j)}{\partial x_j} = \frac{\partial\left[\left(\mu + \frac{\mu t}{\sigma k}\right)\frac{\partial k}{\partial x_j}\right]}{\partial x_j} + G_k + G_b - \rho \varepsilon - Y_M + S_k \tag{5}$$

$$\frac{\partial(\rho \varepsilon)}{\partial t} + \frac{\partial(\rho \varepsilon u_j)}{\partial x_j} = \frac{\partial}{\partial x_j}\left[\left(\mu + \frac{u_t}{\sigma \varepsilon}\right)\frac{\partial \varepsilon}{\partial x_j}\right] + \rho C_1 S_\varepsilon - \rho C_2 \frac{\varepsilon^2}{k + \sqrt{v\varepsilon}} + C_{1\varepsilon}\frac{\varepsilon}{k} C_{3\varepsilon} G_b + S_\varepsilon \tag{6}$$

k and ε are the turbulent kinetic energy and turbulent kinetic energy dissipation rate, respectively, μ_t is the turbulent viscous coefficient, G_k is the turbulent kinetic energy generation rate due to the mean velocity gradient, G_b is the turbulent kinetic energy generation rate due to buoyancy, and Y_M is the dissipation term due to the turbulent pulsating expansion; S_k and S_ε are custom source terms, σ_k and σ_ε are turbulent Prandtl numbers for turbulent kinetic energy and its dissipation rate, respectively, σ_k=1.0 and σ_ε=1.2; C_1 and C_2 are transport dissipation constants, C_1=max $\left(0.43，\right.$

$\frac{\eta}{\eta+5}$), $\eta = \sqrt{2E_{ij} \bullet E_{ij}} \frac{\varepsilon}{k}$, $E_{ij} = \frac{1}{2}\left(\frac{\partial u_i}{\partial x_j} + \frac{\partial u_j}{\partial x_i}\right)$, $C_2=1.9$; $C_{1\varepsilon}$, $C_{3\varepsilon}$ are empirical constants, $C_{1\varepsilon}=1.44$, $C_{3\varepsilon}=0.8$; v is kinematic viscosity.

In this study, the combustion in steel ladle baking is classified as non-premixed gas combustion, utilizing a multi-step reaction mechanism. The reaction rate of the entire chemical process is described using the Eddy Dissipation Concept (EDC) model.

τ^* is the elapsed time scale, Y^* is the mass fraction of the component after the chemical reaction, Y_i represents the concentration of the same substance before the reaction, and ζ^* is the spatial resolution of the small vortex.

Radiative heat transfer is one of the main modes of heat transfer in high-temperature combustion chambers. In this study, the P-1 radiation model[11] is used for the radiation process. This model accounts for radiative scattering and is more suitable for combustion equipment with large optical thickness and complex geometric structures. Additionally, it requires less time to solve the radiative energy equation, making it well-suited for solving radiative heat transfer in gas combustion processes.

$$\frac{dI(\vec{r},\ \vec{s})}{dx} + (a + \sigma_s)I(\vec{r},\ \vec{s}) = an^2\frac{\sigma T^4}{\pi} + \frac{\sigma_s}{4\pi}\int_0^{4\pi} I\left(\vec{r},\ \overrightarrow{s'}\right)\Phi\left(\vec{s},\overrightarrow{s'}\right)d\Omega' \qquad (8)$$

where I is the radiation intensity; $\vec{r}$ is the position vector; $\vec{s}$ is the direction vector; a is the absorption coefficient; σ_s is the scattering coefficient; n is the refraction coefficient; σ is the Steven Boltzmann constant; $\overrightarrow{s'}$ is the direction of scattering; s is the stroke length; Φ is the phase function; Ω' is the volume angle of space.

2.2. Geometric model

The geometry of the ladle is illustrated in Fig. 1, where it is segmented into three distinct layers: a working layer, a permanent layer, and an adiabatic layer. Additionally, Table 1 presents the specific physical parameters of the refractory materials used. The 100-ton steel ladle baking device has been streamlined into a cylindrical structure, featuring a height of 4060 mm and a lid diameter of 3442 mm for enhanced simplicity and efficiency. The baking process employs the utilization of oxygen-fuel combustion. The oxygen-fuel combustion burner for baking is simplified as a circular velocity inlet. Modeled using Space Claim and meshed using Workbench meshing. The baking process utilizes coke oven gas as its fuel source, maintaining a fuel flow rate of 900 cubic meters per hour. The precise compositional breakdown of this fuel is comprehensively outlined in Table 2. As depicted in Fig. 1(a), six monitoring points are positioned on the interior wall of the ladle. The monitoring point d0 is situated precisely at the center of the ladle's bottom, while d1 is positioned at the intersection of the ladle's bottom and wall. Furthermore, d2, d3, d4, and d5 are strategically located on the ladle wall, each positioned at distances of 1.395 meters, 2.395 meters, 3.395 meters, and 4.05 meters respectively, from the base of the ladle.
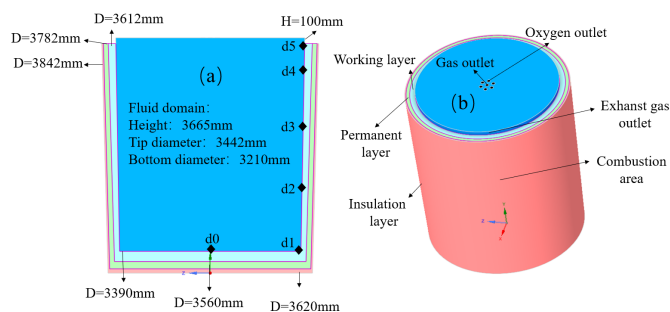

Fig. 1. Schematic diagram of ladle structure (a) Dimensional structure (b) Computational geometric modeling

Table 1.
Physical parameters of refractory materials

Layers	Material	Ladle wall position thickness/mm	Ladle bottom position thickness /mm	Density（Kg/m³）	Specific heat capacity (J/(Kg·K))	Coefficient of thermal conductivity (W/(m·K))
Working layer	Magnesium-carbon brick	270	180	2900	750	2.1
Permanent layer	High aluminum brick	170	130	2380	857	1.22
Insulation layer	SM490B	60	85	7830	480	56

Table 2.
Table of Coke Oven Gas Composition (Volume Fraction)

CH₄	CO	CO₂	H₂	N₂	C₂H₄	C₂H₆	C₃H₆	O₂
26.65	6.29	1.93	59.47	2.16	2.21	0.76	0.2	0.32

2.3. Boundary conditions and operating parameters

The ambient pressure measures 101,325 Pa, with an initial ambient temperature of 300 K, a fuel temperature also at 300 K, and an oxygen temperature significantly higher at 1273 K. The combustion-supporting gas is pure oxygen. Different inlet velocities are set according to the flow rate of the fuel gas. The specific parameters are detailed in Table 3:

Table 3.
Inlet velocities corresponding to different fuel gas pipe diameters

scheme	Fuel gas pipe Diameter(mm)	Oxygen pipe Diameter(mm)	Fuel gas velocity(m/s)	Oxygen velocity(m/s)
I	100	60	31.83	14.73
II	120	60	22.10	14.73
III	150	60	14.14	14.73
IV	180	60	9.82	14.73

After a comprehensive comparison and analysis of four distinct fuel gas diameters, the nozzle spacing was meticulously adjusted to achieve the optimal operating condition, subsequently undergoing numerical simulation while maintaining all other parameters constant. The four conditions are enumerated as follows: V for a spacing of 125 mm, VI for a spacing of 150 mm, VII for a spacing of 175 mm, and VIII for a spacing of 200 mm.

2.4. Grid Independence Verification

The computational domain is a circumferentially symmetric structure, taking 1/6 of the ladle for meshing, and establishing the coordinate axes with the center of the inner bottom surface of the ladle as the center of the circle, as shown in Fig. 2. The grid-independence validation is presented in Fig. 3, revealing that upon exceeding 490,000 grids, the temperature recorded at the central monitoring point at the bottom of the ladle remains virtually constant. Consequently, a grid count of 490,000 is conclusively determined to balance computational accuracy with resource efficiency.
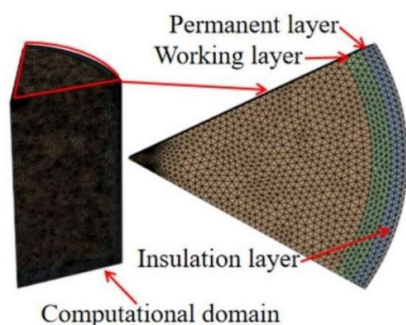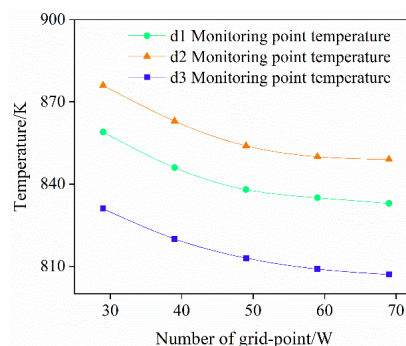

Fig. 2. Computational domain grid

Fig. 3. Verification of grid-independence

2.5. Model validation

Given the challenges in acquiring coke oven gas, natural gas is utilized in this study for model validation purposes. The detailed experimental setup is illustrated in Fig. 4, the size ratio of this ladle model to the experimental model stands at 3:1, with the model boasting a height of 1221mm, a bottom diameter of 1070mm, and a top diameter of 1147mm, featuring the deployment of thermocouples at six strategic monitoring stations. For simulating the behavior of natural gas, Fluent software is employed. The subsequent comparison between the simulated temperatures and the actual temperatures recorded at each monitoring point is presented in Table 4. Upon comparison, it was observed that the temperature at the juncture between the wall and the base of the steel ladle was slightly lower. Conversely, the temperature within the remaining portion of the ladle undergoes a gradual decline, proceeding from the bottom upwards. This phenomenon arises due to the formation of 'dead zones' in the corners, impeding efficient heat transfer. Furthermore, the d0 monitoring point exhibits the highest relative error, stemming from its positioning at the very center of the ladle's bottom, where flame segregation during the combustion process likely occurred. After a comprehensive analysis, the relative errors are found to lie within an acceptable range, thereby suggesting the feasibility of applying the mathematical model for subsequent simulation studies.
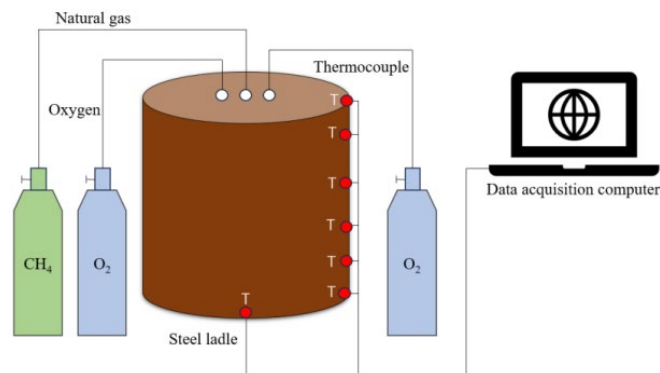
Fig. 4 Schematic diagram of the experiment

Table 4
Measured and simulated values

temperature measurement point	d0	d1	d2	d3	d4	d5
measured value /K	1558	1476	1483	1467	1435	1396
analog value /K	1405	1349	1365	1345	1313	1282
relative error /%	-9.8	-8.6	-7.9	-8.3	-8.5	-8.1

3. Results and discussion

3.1. The impact of different fuel gas velocities on the effectiveness of steel ladle preheating

1) Comparison of flame shapes under different fuel gas velocities

Fig. 5 shows the flame shapes under different fuel gas velocities. It can be seen that after the fuel gas and oxygen are ejected from the nozzle, a stable flame forms after a certain distance. The flame subsequently reaches the base of the ladle and commences to disperse gradually towards the walls of the ladle. The shapes of the flames in the four conditions are largely comparable and exhibit general similarities. From the viewpoint of flame width, the midsection measurements of the flames under the four distinct conditions are 0.39m, 0.42m, 0.46m, and 0.47m, respectively. This implies that when the velocity of the fuel gas is inferior to that of oxygen, a more optimal flame shape is achieved.
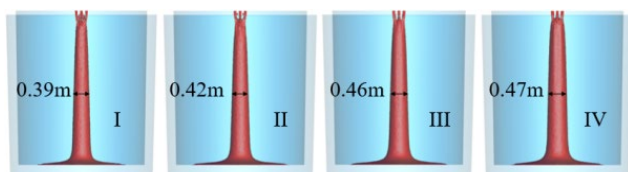

Fig. 5. Comparison of flame shapes under different fuel gas velocities

2) The impact of different fuel gas velocities on the flow field inside the steel ladle

Coke oven gas and oxygen are introduced into the combustion zone via the nozzle, creating a turbulent flow. The distribution of flow fields under the four conditions is depicted in Fig. 6. It is evident that the gas within the furnace creates a substantial recirculation zone within the confines of the steel ladle. The coke oven gas jet and oxygen jet vigorously intertwine and gradually develop into intricate vortices. The majority of the high-temperature flue gas is channelled within these vortices, prolonging its residence time within the ladle, thereby diminishing emissions and enhancing heat transfer efficiency. This additionally aids in preventing the emergence of localized high-temperature zones at the nozzle. The fuel gas velocities in conditions I and II surpass those in conditions III and IV, consequently yielding more concentrated streamlines within the respective areas. Furthermore, in scenarios I and II, the velocity of the fuel gas at the inlet surpasses that of oxygen, consequently resulting in a decreased pressure at the center. This directs the combustion-supporting gas towards the center, leading to denser streamlines at the base.
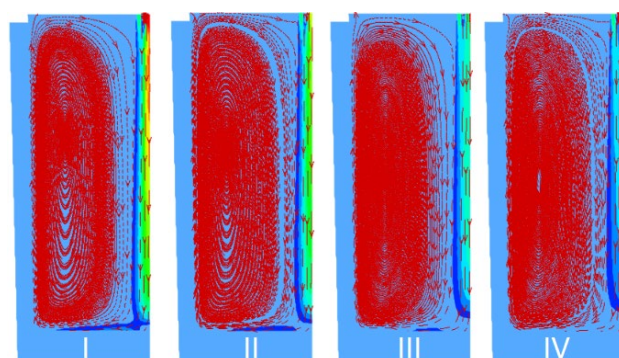

Fig. 6. Flow field distributions under different fuel gas velocities

3) The Impact of Different Fuel Gas Velocities on the Temperature Field Inside a Steel Ladle

Numerical simulations were conducted for scenarios I, II, III, and IV, all under identical baking conditions, with a total cumulative baking time of 10 h. Fig. 7 presents the cloud plots illustrating the temperature distribution over periods of 1 hour and

10 hours, respectively. An examination of the temperature distribution spanning an hour reveals a greater uniformity in the baking temperatures under conditions III and IV. Quantitative analysis reveals that under conditions I-IV, the heights of the regions where temperatures dip below 700K are 3.11m, 2.89m, 2.45m, and 2.45m, respectively. Hence, the area occupied by regions with temperatures beneath 700K under conditions I and II is more extensive. This could potentially be attributed to the fact that the velocity of the fuel gas in conditions I and II surpasses that of the oxygen. As a consequence, the fuel fails to adequately blend with the oxygen prior to circulating within the ladle, thereby resulting in suboptimal baking performance. Upon scrutinizing the temperature distribution in zones exceeding 1000K at the 10th hour mark, it becomes evident that the temperature increase aligns with the directional flow of the flue gas. Specifically, the temperature escalates from the central point of the ladle's base, progressing towards the lateral walls, and subsequently, from the base of these walls to their uppermost sections. In conditions I-IV, the heights of the regions near the ladle wall with temperatures above 1000K are 3.13m, 3.47m, 3.65m, and 3.09m, respectively. The high-temperature region in condition IV is the shortest, attributed to the reduced oxygen velocity. As a consequence, the ejected fuel lacks sufficient oxygen to mix and undergo combustion, ultimately resulting in suboptimal baking performance.
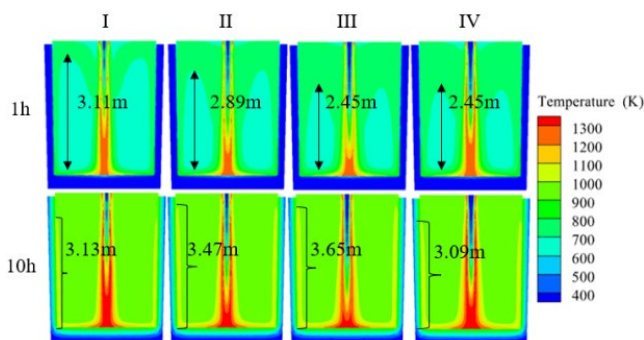

Fig. 7. Temperature field distribution at different fuel gas velocities

4) The Impact of Different Fuel Gas Velocities on the Temperature at the Bottom of the Ladle

Fig. 8 shows the bottom center linear velocity distribution after baking for 2 h. Upon analysis, it is evident that the overall fluid velocity magnitudes for the four conditions adhere to the sequence of $V_I > V_{II} > V_{III} > V_{IV}$, exhibiting a trend of initially increasing and subsequently decreasing. Notably, the temperature attains its peak within the interval of 300-600mm, thereafter commencing a decline. This is due to the deviation of the fuel gas and oxygen towards the sidewalls of the ladle, prior to reaching the bottom. As the diameter expands, the velocity diminishes, resulting in a shift of the initial point of deviation towards the side walls to a higher position. The location at which they arrive at the bottom is situated closer to the lateral walls. Hence, the velocity along the central axis of the bottom reaches its peak within the range of 300 to 600 millimeters. As the velocity diminishes, the location of the peak velocity along the central axis of the bottom shifts towards the lateral walls.
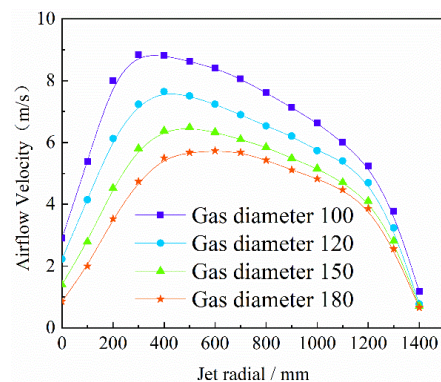

Fig. 8. Bottom centerline velocity

Fig. 9 illustrates the temperatures recorded at the centerline of the ladle's bottom, after 2 hours of baking, for the four operational conditions. It is observable that the temperature undergoes a gradual decline along the centerline, extending from the bottom central point towards the furnace wall. This is due to the flame directly to the bottom of the packet, and in the center of the bottom of the packet began to dissipate heat, in the process of flowing to the packet wall, high-temperature flue gas is constantly exchanging heat with the bottom of the furnace, in the process of exchanging heat, high-temperature flue gas itself will continue to reduce the heat, so the overall trend is declining. The comparative magnitude of temperatures across the four conditions can be expressed as: $T_{III} > T_{II} \geqslant T_{IV} > T_I$. This suggests that adopting Scheme III for baking yields superior temperature outcomes at the base of the furnace.
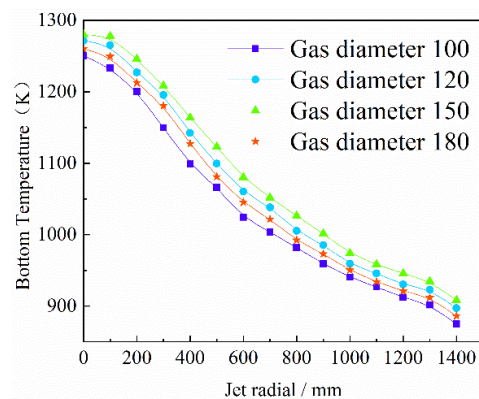

Fig. 9. Bottom centerline temperature

Fig. 10 illustrates the Contour Plot depicting the distribution of Bottom Temperature at varying Fuel Gas Velocities. One can observe that the high-temperature region's area is progressively expanding along the bottom center throughout the 1-10-hour baking process. Considering Scheme III as a representative case, a statistical examination of the temperature domain exceeding 1200K reveals that the diameters of the high-temperature zones at 1h, 4h, 6h, and 10h are respectively 0.6m, 0.8m, 0.96m, and 1.53m. This is attributed to the initial baking phase, during which the temperature inside the bag is not uniformly distributed. As the baking progresses, the temperature within the ladle gradually becomes more uniform, and the heat within the ladle intensifies,

accumulating significantly within the bag. Consequently, the bottom of the ladle experiences a faster rate of temperature increase. Statistics 10h baking moment, four programs in the bottom of the ladle 1200K above the temperature region, can be found in the four programs of the high temperature zone diameter of 1.33, 1.38, 1.53, 1.38m, respectively, the program III of the 1200K temperature area is the largest, the bottom of the ladle baking effect is best.
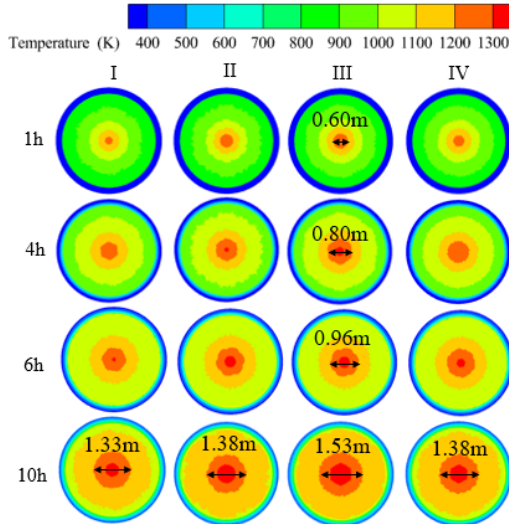

Fig. 10 Contour plot of bottom temperature distribution at different fuel gas velocities

5) The Impact of Different Fuel Gas Velocities on the Temperature of the Inner Wall of the Steel Ladle

Fig. 11 illustrates the temperature distribution across the inner wall surface of the ladle following a 4-hour baking process. Upon observation, it is evident that the temperature ranking of the four schemes follows the order: $T_{III} > T_{II} > T_{IV} > T_I$. Using the ladle wall temperature at 250mm as a case in point, the temperatures for the four respective schemes are 947K, 965K, 966K, and 949K. This once again underscores that the optimal baking effect on the steel ladle wall arises when the velocity of the fuel gas closely aligns with that of the oxygen. The temperature pattern observed on the inner wall surface, across the four scenarios, exhibits an initial rise, followed by a decline, as it traverses from the bottom to the top of the ladle, attaining its peak value roughly at 250 mm. This occurs due to the formation of vortices, also known as 'dead zones,' in the corners where the bottom and wall of the ladle meet. When the high-temperature flue gas reaches the ladle wall, it fails to fully circulate within that specific region. Furthermore, as it approaches the 'dead zones,' the heat transfer becomes increasingly inefficient. Therefore, a temperature rise is observed in the 0-250mm range. A significant quantity of high-temperature flue gas will directly ascend to a height of 250mm, whereupon it commences its upward flow. During this process, a portion of the heat is transferred to the walls of the ladle, causing the temperature of the high-temperature flue gas to diminish. Consequently, a subsequent gradual decrease in the temperature of the ladle wall is observed.
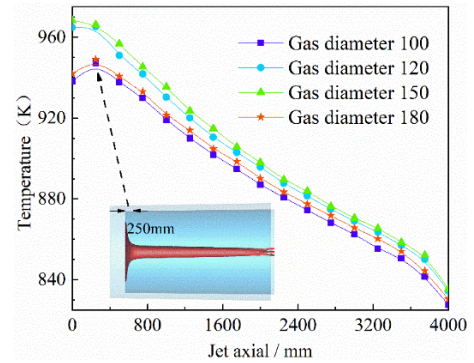

Fig. 11. Radial temperature of the inner wall surface over 4h at different fuel gas velocity

Fig. 12 (a-d) illustrates the temperature distribution across six monitoring points under four distinct working conditions. Comparative analysis reveals that monitoring point d0 exhibits a notably elevated temperature compared to the remaining five points. Specifically, the temperatures at monitoring point d0 under these four conditions reach 1223K, 1244K, 1251K, and 1218K, respectively. This is due to the fact that point d0 is located in the center of the bottom of the ladle, and after the high temperature flue gas reaches the bottom, it first contacts the d0 monitoring point, so the d0 monitoring point has the highest temperature among all the monitoring points. The comparative temperature relationship among d1, d2, and the other monitoring points can be expressed as $T_{d1(d2)} > T_{d3} > T_{d4} > T_{d5}$. When the fuel gas velocity is greater than the oxygen velocity, the temperature at monitoring point d1 is higher than at monitoring point d2. Conversely, when the fuel gas velocity is less than the oxygen velocity, the temperature at monitoring point d1 is lower than at monitoring point d2. Based on this observation, one can deduce that as the nozzle diameter enlarges, there is a corresponding decrease in the gas flow rate, accompanied by a reduction in the 'dead zone' area. Upon comparing the temperatures recorded at various monitoring points under diverse conditions, it becomes evident that the baking effect attains its optimum level when the velocity of the fuel gas is maintained at a nearly 1:1 ratio with the velocity of oxygen. Furthermore, if the velocity of the fuel gas deviates significantly from that of the oxygen, either by being excessively higher or lower, it adversely impacts the steel ladle baking process.
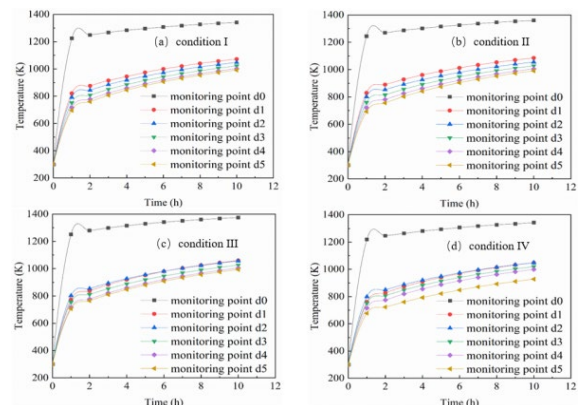

Fig. 12. Temperature line graph of monitoring points

3.2. Influence of different nozzle spacing on the baking effect of ladle

Based on the analysis of the effects of different fuel gas velocities on the steel ladle baking process, further exploration of the impact of different nozzle spacings on the baking effect is conducted. Using Condition III as the baseline, the spacing between the gas nozzles is varied. The corresponding four conditions are: V: spacing 125mm, VI (same as III): spacing 150mm, VII: spacing 175mm, VIII: spacing 200mm.

1) Effect of different nozzle spacing on temperature distribution in ladle

Fig. 13 depicts the temperature distribution across varying nozzle spacings. Upon analyzing the temperature profile within the ladle after an hour of baking, it is evident that the depth of the low-temperature zone, below 700K, measures 2.34m, 2.45m, 2.34m, and 2.44m, respectively. Notably, the variations in width are insignificant, whereas the area sizes exhibit a trend of $S_V \approx S_{VII} < S_{VIII} < S_{VI}$. This suggests that conditions V and VII achieve higher baking efficiency and better temperature uniformity within the initial hour.

Furthermore, examining the area above 1200K at the flame reveals an inverse relationship with nozzle spacing, as indicated by $S_V > S_{VI} > S_{VII} > S_{VIII}$. This indicates that as the nozzle spacing increases, the area occupied by the high-temperature region at the flame diminishes. Upon examining the temperature distribution within the ladle after a 10-hour baking period, it is evident that the regions adjacent to the ladle wall, with temperatures exceeding 1000K, attain heights of 3.38m, 3.65m, 3.58m, and 3.51m, respectively. In terms of area comparison, the sequence is as follows: $S_{VI} > S_{VII} > S_{VIII} > S_V$. Consequently, when the spout spacing is situated within the range of 150mm to 175mm, it yields an optimal baking effect on the ladle wall, and fine-tuning the spout spacing within this range minimally impacts the overall baking efficiency on the wall.
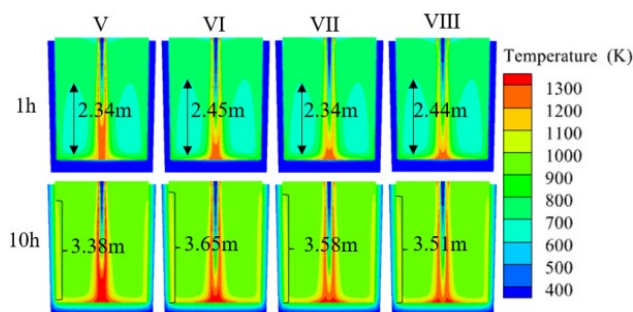
study, quantitative analysis of the bottom temperature distribution under Condition VII at distinct time intervals reveals that the diameters of this region at 1, 4, 8, and 10 hours are 0.48m, 0.82m, 1.33m, and 1.52m, respectively.

Notably, the rate of temperature increase in the high-temperature zone between 1 and 4 hours is inferior to that observed between 4 and 8 hours. This disparity stems from the initial unevenness of the temperature distribution within the ladle during the early baking stages. Initially, the circulation zone lacks significant volumes of high-temperature flue gas, resulting in a relatively low temperature. Consequently, the influx of high-temperature flue gas into the circulation zone is substantial but fleeting, with limited residence time at the base.

As the baking progresses, the temperature distribution within the ladle homogenizes, facilitating the accumulation of substantial amounts of high-temperature flue gas in the circulation zone. This leads to an intensified heat transfer to the base, explaining why the rate of temperature increase is more pronounced between 4 and 8 hours compared to the initial 1 to 4 hours period. By concurrently analyzing the high-temperature areas (S) of the four conditions over an identical time span, it becomes evident that $S_{VI} > S_{VII} > S_{VIII} > S_V$. Notably, Condition V exhibits a substantially smaller area compared to the others, stemming from the significant accumulation of high-temperature flue gas within the flame zone between the inlet and the ladle bottom's center, with only a minimal portion reaching the bottom directly. Consequently, the baking effect on the ladle bottom is inferior in Condition V.

Furthermore, when contrasting the maximum temperatures (T_{max}) at the bottom center across various schemes, it is discernible that the maximum temperature at the ladle's bottom center in Scheme VIII is a notably lower 1304K, significantly trailing behind the other schemes. This phenomenon could be attributed to the wider nozzle spacing, which prompts the flame to divert towards the ladle wall before reaching the bottom center. In conclusion, the baking efficiency at the ladle's bottom is optimized when the nozzles are spaced between 150 and 175 mm.
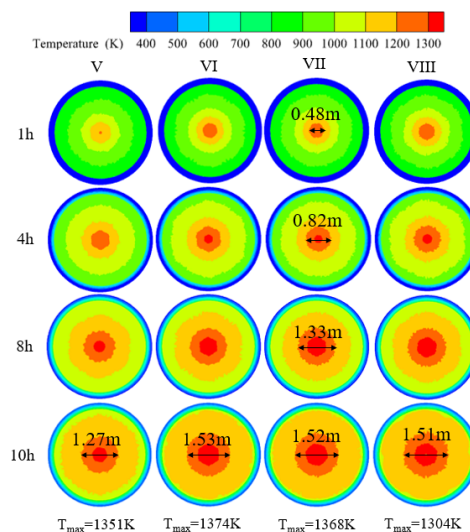

Fig. 13. Temperature field distribution for different nozzle spacing

2) The Effect of Different Nozzle Spacings on the Temperature at the Bottom of the Steel Ladle

Fig. 14 depicts the temperature distribution at the base of the ladle, showcasing distinct patterns for varying nozzle spacings. It is evident that as the baking process advances, the area experiencing temperatures exceeding 1200K progressively expands. Focusing on the 1200K temperature region as a case

Fig. 14. Temperature distribution of the bottom disk for different nozzle spacing

3) The Effect of Different Nozzle Spacings on the Velocity and Temperature Along the Centerline of the Bottom

Fig. 15 illustrates the linear velocities recorded at the bottom center during the baking process for 2 hours, across four distinct working conditions. Notably, Condition V consistently exhibits the lowest velocity throughout the entire baking cycle. For the remaining three conditions, the velocity patterns within the 500-600mm range exhibit variations. Specifically, below 500mm, velocities are inversely proportional to spacing, whereas above 600mm, larger spacings correspond to higher velocities. This phenomenon arises due to the shift in the location where high-temperature flue gas reaches the ladle's bottom, moving closer to the wall as spacing increases. Consequently, the peak velocity point migrates towards the ladle wall, altering the velocity relationships within the 500-600mm range. Overall, the velocity trend exhibits an initial increase followed by a decline. Within the 0-500mm range, the velocity consistently escalates, attributable to the rapid decrease in vertical velocity as fuel and oxygen reach the bottom, partially converting into horizontal velocity. As the flow progresses from the bottom center towards the ladle wall, inertial forces accelerate the velocity within the 0-500mm zone. However, beyond this point, viscous forces and continuous friction contribute to energy dissipation, ultimately resulting in a velocity decrease. Fig. 16 depicts the temperature profile along the bottom centerline at the 2-hour mark. It is evident that the temperature gradually diminishes from the center of the bottom towards the furnace periphery. Specifically, at the 500mm location, the temperatures under the four conditions are 1071K, 1122K, 1113K, and 1096K, respectively. The temperature hierarchy follows as $T_{VII} > T_{VIII} > T_I > T_V$, suggesting that a nozzle spacing ranging from 150mm to 175mm yields superior baking outcomes for the bottom region.
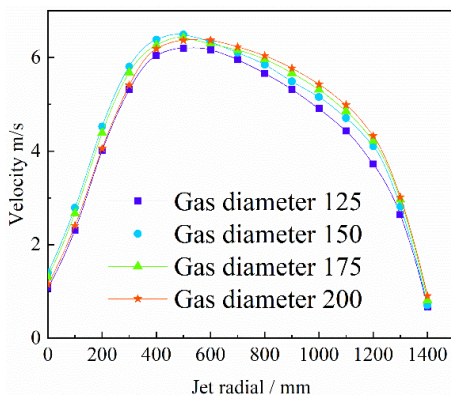

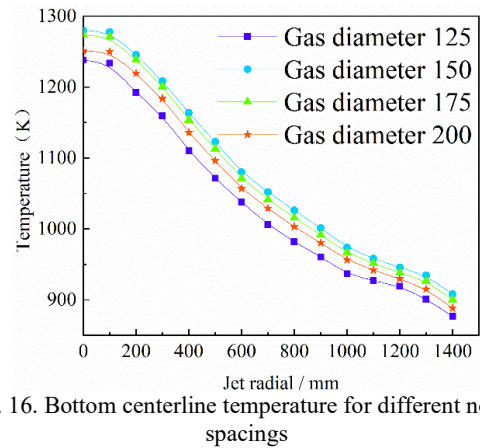Fig. 15. Bottom centerline velocity for different nozzle spacings

Fig. 16. Bottom centerline temperature for different nozzle spacings

4) Effect of different spacing on wall temperature

Fig. 17 illustrates the comparative outcomes of the four operational scenarios in terms of the 4-hour internal wall surface temperature trends. These trends exhibit an initial rise followed by a decline, primarily attributed to the presence of a "dead zone." The proximity to this "dead zone" negatively correlates with the effectiveness of heat transfer, resulting in diminished performance.

Comparing the temperatures across the four conditions, the ranking is as follows: $T_{VI} > T_{VII} > T_{VIII} > T_V$. Taking the temperature at 250mm as a representative example, the corresponding temperatures for these conditions are 954K, 966K, 963K, and 956K, respectively. This signifies that when the spacing between nozzles falls within the range of 150-175mm, a superior baking effect is achieved on the internal wall surface.
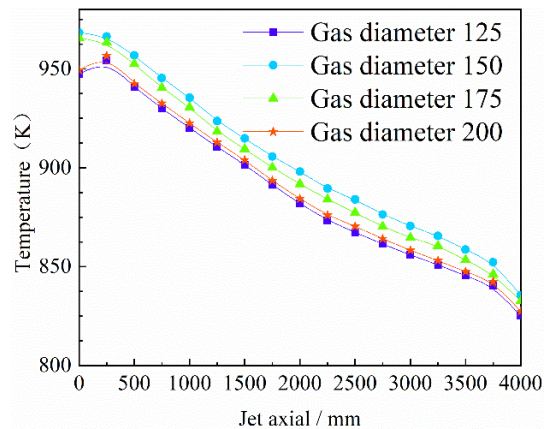

Fig. 17. Temperature Distribution on the Inner Single Wall Surface at Different Nozzle Spacings

3.3. Comparison of thermal efficiency under different operating conditions

The thermal efficiencies for the eight operating conditions were calculated with the following equations:

$$\eta = \frac{Q'}{Q_1+Q_2} \times 100\% \tag{9}$$

Where: η is the thermal efficiency of the ladle baking system; Q' is the volumetric heat storage of the ladle lining and shell, kJ/h; Q_1 is the chemical heat of fuel combustion, kJ/h; and Q_2 is the physical heat brought in by combustion-assisting oxygen, kJ/h.

$$Q' = \sum m_i C_i (t_w - t_0) \tag{10}$$

$$Q_1 = BQ\tau_l \tag{11}$$

$$Q_2 = B(C_k t_k - C_{kc} t_c) \tag{12}$$

Where: m_i is the mass of each layer of material of ladle lining and shell, kg; C_i represents the specific heat capacity of each layer of materials in the ladle lining and shell, measured in kJ/kg°C; τ_l is the ladle baking time, h; t_w is the average temperature of the ladle lining and shell at the moment τ_l; t_0 is the average temperature of the inner and outer walls of the ladle lining and shell at the beginning of baking; B is the fuel usage, m3/h; Q is the received base low (bit) heat generation of the fuel, kJ/m³; C_k and C_{kc} represent the average specific heat capacity of oxygen between 0 to t_k and t_c, measured in kJ/m³°C; t_k is the air temperature; t_c is the ambient temperature.

This model has a total of three layers of ladle shells, from the inside to the outside, respectively, the working layer, the permanent layer, and the adiabatic layer, and the final average temperatures of the inner and outer walls of the eight operating conditions and the calculated thermal efficiencies are shown in Fig. 18.

Fig. 18 illustrates the average temperature of each working layer of the inner and outer walls after 10 hours of baking, as well as the corresponding baking thermal efficiency. It is evident that the average thermal efficiency under the eight conditions is only 22.77%, indicating significant potential for improvement in the efficiency of oxygen-fuel combustion baking of steel ladles. The average temperatures of the working, permanent, and insulating layers were 761.4 K, 513.1 K, and 406.4 K, respectively. Upon comparing the baking temperatures of working conditions I, II, III and IV, it was found that the temperatures of the working layer, permanent layer and insulating layer in working condition III can reach 779.6 K, 528.4 K and 421.7 K respectively with a corresponding thermal efficiency reaching up to 24.33%. This represents an increase in thermal efficiency by about 1.16% to 2.77% compared to other three working condition points. Similarly when comparing efficiencies between working conditions V, VII, VIII and VI(III), it was observed that VI(III) has a higher thermal efficiency by approximately 1% to 2 .61 % compared to other three conditions.

Based on the fuel gas pipeline diameter in Condition III, changes in the nozzle spacing of the fuel gas will also result in variations in baking temperature and efficiency. In other words, optimizing both the fuel gas pipeline diameter and nozzle spacing can enhance baking temperature and efficiency. Specifically, under conditions where the gas diameter is altered, the highest baking thermal efficiency was achieved with a gas nozzle diameter of 150 mm, at 24.33%, while the lowest was recorded with a gas nozzle diameter of 100 mm, at 21.55%. When adjusting the nozzle spacing, the highest baking thermal efficiency was observed at a nozzle spacing of 150mm, reaching an efficiency of 24.33%, whereas it dropped to its lowest point at a nozzle spacing of 125mm, with an efficiency of 21.71%.
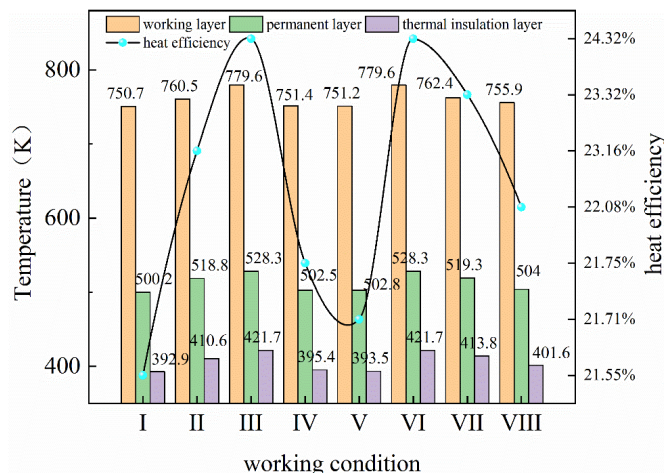

Fig. 18. Final Average Temperature and Thermal Efficiency of Inner and Outer Walls

4. Conclusion

This paper conducts a numerical simulation study on the process of baking a 100t ladle using oxygen-fuel combustion. The focus is on analyzing the baking effect of oxygen velocity and the spacing of the nozzles for oxygen and gas on the ladle. The following conclusions are drawn: -

In terms of fuel gas velocity, it is found that when the velocity is significantly higher or lower than the oxygen velocity, it is not conducive to steel ladle baking. The best baking results are achieved when the fuel gas velocity is approximately equal to the oxygen velocity.

The temperature trend of the inner wall surface of the ladle shows an increase followed by a decrease from bottom to top, reaching its maximum value at a height of about 250 mm.

Regarding nozzle spacing, it is observed that when the spacing between the fuel gas nozzle and the oxygen nozzle falls within 150mm to 175mm range, better baking effects are achieved both at bottom and wall of ladle.

Amongst eight design options simulated in this study, it was found that highest baking efficiency (24.33%) can be achieved with a gas pipeline diameter of 150 mm, an oxygen pipeline diameter of 60 mm, and a spacing between gas nozzle and oxygen nozzle set at 150 mm.

Acknowledgments

References

[1] Li, G., Liu, J., Jiang, G. & Liu, H. (2015). Numerical simulation of temperature field and thermal stress field in the new type of ladle with the nanometer adiabatic material. *Advances in Mechanical Engineering*. 7(4), 1-13. https://doi.org/10.1177/1687814015575988.

[2] Peng, L., Yu, J., Zhao, H., Zhang, H. & Ziheng, S. (2023). Preliminary Investigation on the application of a semi-lightweight mullite spherical solid waste material in ladle permanent layer. *Transactions of the Indian Ceramic Society*. 82(4), 287-294. https://doi.org/10.1080/0371750x.2023.2260848.

[3] Yuan, F., He, D., Feng, K., Zhang, M. & Wang, H. (2018). Optimal design and experimental study of ejector for ladle baking. *Steel Research International*. 89(12), 1800051. https://doi.org/10.1002/srin.201800051.

[4] Deng, S., Xu, A., Yang, G. & Wang, H. (2018). Analyses and calculation of steel scrap melting in a multifunctional hot metal ladle. *Steel Research International*. 90(3), 18000435. https://doi.org/10.1002/srin.201800435.

[5] Bělohradský, P., Skryja, P. & Hudák, I. (2014). Experimental study on the influence of oxygen content in the combustion air on the combustion characteristics. *Energy*. 75, 116-126. https://doi.org/10.1016/j.energy.2014.04.026.

[6] Nemitallah, M.A., Habib, M.A., Badr, H.M., Said, S.A., Jamal, A., Ben-Mansour, R., Mokheimer, E.M.A. & Mezghani, K. (2017). Oxy-fuel combustion technology: current status, applications, and trends. *International Journal of Energy Research*. 41(12), 1670-1708. https://doi.org/10.1002/er.3722.

[7] Liu, W., Zuo, H., Wang, J., Xue, Q., Ren, B. & Yang, F. (2021). The production and application of hydrogen in steel industry. *International Journal of Hydrogen Energy*. 46(17), 10548-10569. https://doi.org/10.1016/j.ijhydene.2020.12.123.

[8] Xie, W., Ma, J., Wang, D., Liu, Z. & Yang, A. (2024). Research on the carbon reduction technology path of the iron and steel industry based on a multi-objective genetic algorithm. *Sustainability*. 16(7), 2966, 1-30. https://doi.org/10.3390/su16072966.

[9] Löschau, M. (2018). Effects of combustion temperature on air emissions and support fuel consumption in full scale fluidized bed sludge incineration: with particular focus on nitrogen oxides and total organic carbon. *Waste Management & Research: The Journal for a Sustainable Circular Economy*. 36(4), 342-350. https://doi.org/10.1177/0734242x18755895.

[10] Tian, Y., Yang, S., Le, J., Zhong, F. & Tian, X. (2017). Investigation of combustion process of a kerosene fueled combustor with air throttling. *Combustion and Flame*. 179, 74-85. https://doi.org/10.1016/j.combustflame.2017.01.021.

[11] Yuan, F., Wang, H.-B., Zhou, P.-L. & Xu, A.-J. (2018). Combustion performance of nozzles with multiple gas orifices in large ladles for temperature uniformity. *Journal of Iron and Steel Research International*. 25(4), 387-397. https://doi.org/10.1007/s42243-018-0048-9.

[12] Moradi, J., Gharehghani, A. & Mirsalim, M. (2020). Numerical investigation on the effect of oxygen in combustion characteristics and to extend low load operating range of a natural-gas HCCI engine. *Applied Energy*. 276, 115516. https://doi.org/10.1016/j.apenergy.2020.115516.

[13] Shan, S., Chen, B., Zhou, Z. & Zhang, Y. (2022). A review on fundmental research of oxy-coal combustion technology. *Thermal Science*. 26(2C), 1945-1958. https://doi.org/10.2298/tsci210329238s.

[14] Shi, B., Hu, J. & Ishizuka, S. (2015). Carbon dioxide diluted methane/oxygen combustion in a rapidly mixed tubular flame burner. *Combustion and Flame*. 162(2), 420-430. https://doi.org/10.1016/j.combustflame.2014.07.022.

[15] Wang, H., Lei, Q., Li, P., Liu, C., Xue, Y., Zhang, X., Li, C. & Yang, Z. (2021). Key CO2 capture technology of pure oxygen exhaust gas combustion for syngas-fueled high-temperature fuel cells. *International Journal of Coal Science & Technology*. 8(3), 383-393. https://doi.org/10.1007/s40789-021-00445-1.

[16] Toftegaard, M.B., Brix, J., Jensen, P.A. Glarborg, P. & Jensen, A.D. (2010). Oxy-fuel combustion of solid fuels. *Progress in Energy and Combustion Science*. 36(5), 581-625. https://doi.org/10.1016/j.pecs.2010.02.001.

[17] Jovanovic, R., Swiatkowski, B., Kakietek, S., Škobalj, P., Lazović, I. & Cvetinovic, D. (2019). Mathematical modelling of swirl oxy-fule burner flame characteristics. *Energy Conversion and Management*. 191, 193-207. https://doi.org/10.1016/j.enconman.2019.04.027.

[18] Gao, K., Ke, X., Du, B., Wang, Z., Jin, Y., Huang, Z., Li, Y. & Liu, X. (2024). Simulation of gas–solid flow characteristics of the circulating fluidized bed boiler under pure-oxygen combustion conditions. *Chinese Journal of Chemical Engineering*. 70, 9-19. https://doi.org/10.1016/j.cjche.2024.02.008.

[19] Shi, B., Shimokuri, D. & Ishizuka, S. (2014). Reexamination on methane/oxygen combustion in a rapidly mixed type tubular flame burner. *Combustion and Flame*. 161(5), 1310-1325. https://doi.org/10.1016/j.combustflame.2013.11.001.

[20] Zhuang, S., Zhan, D., Wang, T., Li, P. & Yang, Y. (2023). Influence of oxy-fuel lance parameters on the scrap pre-heating temperature in the hot metal ladle. *Metals*. 13(5), 1-19. https://doi.org/10.3390/met13050847.

[21] Zhang, H., Zhou, P. & Yuan, F. (2021). Effects of ladle lid or online preheating on heat preservation of ladle linings and temperature drop of molten steel. *Energy*. 214, 118896. https://doi.org/10.1016/j.energy.2020.118896.